Journal of Solid State Chemistry 181 (2008) 3308–3316

Contents lists available at ScienceDirect

Journal of Solid State Chemistry

journal homepage: www.elsevier.com/locate/jssc

Solid chemistry of the Zn^{II}/1,2,4-triazolate/anion system: Separation of 2D isoreticular layers tuned by the terminal counteranions X ($X = Cl^-$, Br^-, I^-, SCN^-)

Sanping Chen, Shu Sun, Shengli Gao *

Department of Chemistry, Key Laboratory of Synthetic and Natural Functional Molecule Chemistry of Ministry of Education, Northwest University, Xi'an, Shaanxi 710069, PR China

ARTICLE INFO

Article history:
Received 30 April 2008
Received in revised form
8 August 2008
Accepted 19 August 2008
Available online 5 September 2008

Keywords:
Zn(II)
1,2,4-Triazole
Coordination polymer
2D layer
Fluorescent emission

ABSTRACT

An array of 2D isoreticular layers, viz. $[Zn(atrz)X]_\infty$ (**1**·*X*; $X = Cl^-$, Br^-, I^-; atrz = 3-amino-1,2,4-triazole anion), $[Zn_4(atrz)_4(SCN)_4 \cdot H_2O]_\infty$ (**1**·SCN·H_2O) and $[Zn(trz)X]_\infty$ (**2**·*X*; $X = Cl^-$, Br^-, I^-; trz = 1,2,4-triazole anion), have been hydrothermally synthesized and structurally characterized. Compounds **1**·*X* and **1**·SCN·H_2O are constructed from binuclear planar $Zn_2(atrz)_2$ subunits and exhibit (4,4) topological network when the subunits are simplified as four-connected nodes. Based on changing the terminal counteranions *X* ($X = Cl^-$, Br^-, I^-, SCN^-), the average interlayer separations of **1**·*X* and **1**·SCN·H_2O are enlarged, which equal to 5.851, 6.153, 6.651 and 8.292 Å, respectively. As a result, H_2O molecules reside in the spaces between two adjacent layers of **1**·SCN·H_2O. **2** and **1** are the isomorphous structures. In common with **1**, the interlayer separations of **2**·*X* are widened with increasing the ion radius. Solid-state luminescence properties and thermogravimetric analyses of **1** and **2** were investigated, respectively.

1. Introduction

During the past decades, organic–inorganic hybrids derived from transitional metal ions and multifunctional bridging ligands have drawn great current interest due to their potential technological applications [1]. Using assembly strategy, prototypical organic–inorganic hybrid materials have been constructed from metal cluster nodes linked through polyfunctional carboxylates, polypyridyl ligands and organodiphosphonate ligands [2–14]. More recently, polyazaheteroaromatic organic ligands such as pyrazole, imidazole, triazole and tetrazole have been employed in the construction of organic–inorganic architectures [15–20].

As the representative of simple organic ligands, in addition to affording different tether lengths, different charge-balance requirements and alternative functional group orientations, 1H-1,2,4-triazole (Htrz) unites the coordination geometries of both pyrazole and imidazole (see Scheme 1), and exhibits a strong and typical property of acting as bridging ligand among metal centers, which provides access to the design and syntheses of the molecular scale composites of inorganic and organic components [18,19,21]. Similarly, 3-amino-1H-1,2,4-triazole (Hatrz), one of 1,2,4-triazole derivatives, possesses all virtues of Htrz, and especially which could be employed as a asymmetrically substituted achiral ligand to build novel chiral compounds when N-ligating donor in the amino group attached to Hatrz participates in coordination. Li et al. [22] obtained a novel chiral cadmium coordination polymer, Cd(atrz)Cl, based on the unsymmetrical achiral atrz anion with an unprecedented μ_4-bridging mode.

The 2D isoreticular layers $[Zn(\mu_3\text{-trz})Cl]_\infty$ were explored by Kröber via slow diffusion of methanol solution in an H-shape tube [23], which was the first entity of the isomeric structures $[Zn(trz)X]_\infty$ ($X = Cl^-$, Br^-) [19,23]. Afterward, four similar 2D corrugated isoreticular networks $[Cu(trz)]_\infty$, $[Ag(trz)]_\infty$, Zn(dmtrz)Cl (dmtrz = 3,5-dimethyl-1,2,4-triazole anion), and Cd(datrz)I (datrz = 3,5-diamino-1,2,4-triazole anion) were reported by Zhang et al. [24] and Zhai et al. [25], respectively. As an extension of the above work, we expect the possible connection channels would be present in the whole crystalloid if the adjacent layers could be regularly overlapped face-to-face. Based on the considerations, zinc triazolate isoreticular layer frameworks, $[Zn(atrz)X]_\infty$ (**1**·*X*; $X = Cl^-$, Br^-, I^-; atrz = 3-amino-1,2,4-triazole anion), $[Zn_4(atrz)_4(SCN)_4 \cdot H_2O]_\infty$ (**1**·SCN·H_2O) and $[Zn(trz)X]_\infty$ (**2**·*X*; $X = Cl^-$, Br^-, I^-; trz = 1,2,4-triazole anion) have been synthesized via a hydrothermal technique in the context. Structural analyses revealed that the average interlayer separations of the targets were enlarged by changing the terminal

* Corresponding author.
E-mail address: gaoshli@nwu.edu.cn (S. Gao).

0022-4596/$ - see front matter © 2008 Elsevier Inc. All rights reserved.
doi:10.1016/j.jssc.2008.08.027

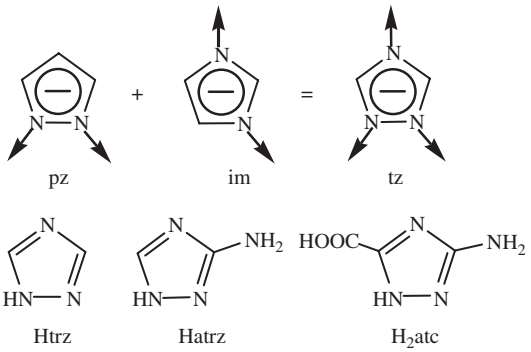

Scheme 1.

coordination counteranions X ($X = Cl^-$, Br^-, I^-, SCN^-). As expected, H_2O molecules reside in the spaces between two adjacent layers of $\mathbf{1}\cdot SCN\cdot H_2O$.

2. Experimental section

2.1. Materials and analytical methods

Commercially available reagents were used as received without further purification. Elemental analyses of C, H, N were performed on a Vario EL III analyzer. Infrared spectra were obtained from KBr pellets within the region 400–4000 cm^{-1} on a BEQ VZNDX 550 FTIR spectrometer. The powder X-ray diffraction (PXRD) was recorded on a Rigaku D/Max-2500 diffractometer at 40 kV, 100 mA for a Cu-target tube and a graphite monochromator. Thermogravimetric measurements were carried out from room temperature to 900 °C for **1** and **2** on preweighed samples in hydrostatic air atmosphere using TA Instruments NETRZSCH STA 449C simultaneous TGA–DSC with a heating rate of 10 °C min^{-1}. Fluorescence spectroscopy data were recorded on a model F-4500 fluorescence spectrophotometer.

2.2. Synthesis

2.2.1. Synthesis of $[Zn(atrz)Cl]_\infty$ ($\mathbf{1}\cdot Cl$)

A mixture of $Zn(NO_3)_2\cdot 6H_2O$ (0.119 g, 0.40 mmol), Hatrz (0.034 g, 0.40 mmol), NH_4Cl (0.021 g, 0.40 mmol) and H_2O (6 g, 333 mmol), was stirred until it was homogeneous, and then sealed in a 8 mL Teflon-lined stainless reactor, kept under autogenous pressure at 160 °C for 72 h, followed by slow cooling down to room temperature by 5 °C/h. Colorless rhombic crystals suitable for X-ray crystal analyses were isolated in 21% yield (based on Zn), which are stable in air and insoluble in water and common organic solvents. IR (KBr pellet, cm^{-1}): ν 3476 m, 3381 m, 3321 w, 3125 w, 1755 w, 1622 s, 1556 s, 1523 s, 1421 m, 1307 m, 1228 m, 1113 w, 1066 m, 1019 w, 879 m, 769 w, 742 m, 642 w, 486 m. Elemental analysis for $\mathbf{1}\cdot Cl$: $C_2H_3N_4ZnCl$ ($M_r = 183.90$). Calcd: H 1.64%, C 13.06%, N 30.46%. Found: H 1.51%, C 13.03%, N 30.54%.

2.2.2. Synthesis of $[Zn(atrz)Br]_\infty$ ($\mathbf{1}\cdot Br$)

A mixture of $Zn(NO_3)_2\cdot 6H_2O$ (0.089 g, 0.30 mmol), 3-amino-5-carboxyl-1,2,4-triazole (H_2atc) (0.055 g, 0.40 mmol), $(Me)_4NBr$ (0.046 g, 0.30 mmol) and H_2O (6 g, 333 mmol), was stirred until it was homogeneous, and then sealed in a 8 mL Teflon-lined stainless reactor, kept under autogenous pressure at 160 °C for 72 h, and then slowly cooled to room temperature at a rate of 5 °C/h. Suitable colorless rhombic crystals, stable in air and insoluble in water and common organic solvents, were isolated in 32% yield (based on Zn). IR (KBr pellet, cm^{-1}): ν 3478 m, 3376 m, 3120 w, 1757 w, 1621 s, 1551 s, 1521 s, 1418 m, 1304 m, 1226 m, 1110 w, 1061 m, 1015 w, 879 m, 766 w, 740 m, 640 w, 484 m. Elemental analysis for $\mathbf{1}\cdot Br$: $C_2H_3N_4ZnBr$ ($M_r = 228.36$). Calcd: H 1.32%, C 10.52%, N 24.53%. Found: H 1.54%, C 10.56%, N 24.64%.

2.2.3. Synthesis of $[Zn(atrz)I]_\infty$ ($\mathbf{1}\cdot I$)

Compound $\mathbf{1}\cdot I$ was prepared following the procedure described for compound $\mathbf{1}\cdot Br$, but KI was used instead of $(Me)_4NBr$. Colorless rhombic crystals, stable in air and insoluble in water and common organic solvents, were isolated in 35% yield (based on Zn). IR (KBr pellet, cm^{-1}): ν 3473 m, 3362 m, 3113 w, 1760 w, 1622 s, 1548 s, 1519 s, 1416 m, 1299 m, 1223 m, 1105 w, 1056 m, 1013 w, 881 m, 765 w, 737 w, 637 w, 479 m. Elemental analysis for $\mathbf{1}\cdot I$: $C_2H_3N_4ZnI$ ($M_r = 275.35$). Calcd: H 1.10%, C 8.72%, N 20.35%. Found: H 1.09%, C 8.75%, N 20.46%.

2.2.4. Synthesis of $[Zn_4(atrz)_4(SCN)_4\cdot H_2O]_\infty$ ($\mathbf{1}\cdot SCN\cdot H_2O$)

A mixture of $Zn(NO_3)_2\cdot 6H_2O$ (0.089 g, 0.30 mmol), Hatrz (0.025 g, 0.30 mmol), NH_4SCN (0.023 g, 0.30 mmol) and H_2O (6 g, 333 mmol), was stirred until it was homogeneous, and then sealed in a 8 mL Teflon-lined stainless reactor, kept under autogenous pressure at 145 °C for 72 h, followed by slow cooling down to room temperature at a rate of 5 °C/h. Colorless and club-shaped crystals, stable in air and insoluble in water and common organic solvents, were isolated in 37% yield (based on Zn). IR (KBr pellet, cm^{-1}): ν 3455 m, 3364 m, 3118 w, 2081 s, 1630 s, 1558 s, 1524 m, 1422 m, 1305 m, 1228 m, 1116 w, 1066 m, 1018 w, 875 m, 770 w, 740 w, 643 w, 482 m. Elemental analysis for $\mathbf{1}\cdot SCN\cdot H_2O$: $C_{12}H_{11}N_{20}S_4Zn_4O$ ($M_r = 841.13$). Calcd: H 1.32%, C 17.14%, N 33.30%. Found: H 1.95%, C 16.40%, N 33.24%.

2.2.5. Synthesis of $[Zn(trz)Cl]_\infty$ ($\mathbf{2}\cdot Cl$)

Compound $\mathbf{2}\cdot Cl$ was prepared following the procedure described for compound $\mathbf{1}\cdot Cl$, except that Htrz (0.028 g, 0.40 mmol) was used instead of Hatrz. Colorless rhombic crystals, stable in air and insoluble in water and common organic solvents, were isolated in 28% yield (based on Zn). IR (KBr pellet, cm^{-1}): ν 3111 m, 3042 w, 2945 w, 1529 s, 1331 w, 1303 s, 1218 w, 1177 s, 1097 s, 1045 m, 1007 s, 885 m, 659 s. Elemental analysis for $\mathbf{2}\cdot Cl$: $C_2H_2N_3ZnCl$ ($M_r = 168.89$). Calcd: H 1.19%, C 14.22%, N 24.88%. Found: H 1.37%, C 14.08%, N 24.56%.

2.2.6. Synthesis of $[Zn(trz)Br]_\infty$ ($\mathbf{2}\cdot Br$)

Compound $\mathbf{2}\cdot Br$ was prepared following the procedure described for compound $\mathbf{2}\cdot Cl$, except that $(Me)_4NBr$ (0.123 g, 0.80 mmol) was used instead of NH_4Cl. Colorless rhombic crystals, stable in air and insoluble in water and common organic solvents, were isolated in 33% yield (based on Zn). IR (KBr pellet, cm^{-1}): ν 3129 w, 3108 m, 3041 w, 2943 w, 1528 s, 1330 w, 1302 s, 1217 w, 1177 m, 1096 s, 1042 m, 1005 m, 902 w, 884 m, 658 s. Elemental analysis for $\mathbf{2}\cdot Br$: $C_2H_2N_3ZnBr$ ($M_r = 213.35$). Calcd: H 0.94%, C 11.26%, N 19.69%. Found: H 0.86%, C 11.28%, N 19.80%.

2.2.7. Synthesis of $[Zn(trz)I]_\infty$ ($\mathbf{2}\cdot I$)

A mixture of $Zn(NO_3)_2\cdot 6H_2O$ (0.119 g, 0.40 mmol), Htrz (0.028 g, 0.40 mmol), KI (0.083 g, 0.50 mmol) and H_2O (6 g, 333 mmol), was stirred until it was homogeneous, and then sealed in a 8 mL Teflon-lined stainless reactor, kept under autogenous pressure at 160 °C for 72 h, and then slowly cooled to room temperature at a rate of 5 °C/h. Colorless prism crystals, stable in air and insoluble in water and common organic solvents, were isolated in 23% yield (based on Zn). IR (KBr pellet, cm^{-1}): ν 3105 m, 3040 w, 2937 w, 1529 s, 1329 w, 1301 s, 1214 w, 1175 s,

Table 1
Summary of crystallographic data for the structures of **1**, **2** · Br and **2** · I

Compound	**1** · Cl	**1** · Br	**1** · I	**1** · SCN · H_2O	**2** · Br	**2** · I
Formula	$C_2H_3N_4ZnCl$	$C_2H_3N_4ZnBr$	$C_2H_3N_4ZnI$	$C_{12}H_{11}N_{20}S_4Zn_4O$	$C_2H_2N_3ZnBr$	$C_2H_2N_3ZnI$
M_n	183.90	228.36	275.35	841.13	213.35	260.34
Temperature (K)	273(2)	273(2)	273(2)	273(2)	273(2)	273(2)
Crystal system	Orthorhombic	Orthorhombic	Orthorhombic	Orthorhombic	Monoclinic	Monoclinic
Space group	*Pbca*	*Pbca*	*Pbca*	*Pcca*	P2(1)/*n*	*P*2(1)/*n*
a (Å)	9.3873(7)	9.399(2)	9.5053(8)	32.201(5)	6.3995(7)	6.8124(6)
b (Å)	10.0992(8)	10.073(3)	9.9892(8)	9.2185(14)	9.6669(10)	9.6285(8
c (Å)	11.7025(9)	12.306(3)	13.3019(11)	10.1085(15)	9.1216(9)	9.5273(8)
α (°)	90	90	90	90	90	90
β (°)	90	90	90	90	103.4350(10)	108.4470(10)
Γ (°)	90	90	90	90	90	90
V (Å^3)	1109.45(15)	1165.1(5)	1263.02(18)	3000.7(8)	548.85(10)	592.82(9)
Z	8	8	8	4	4	4
F(000)	720	864	1008	1660	400	472
P_{calcd} (g/cm^3)	2.202	2.604	2.896	1.862	2.582	2.917
μ (mm^{-1})	4.789	10.961	8.673	3.484	11.619	9.226
Data/restraints/param	981/0/74	1028/2/77	1116/0/74	2649/0/195	1243/0/65	1043/0/65
GOF	1.086	1.027	1.043	0.925	1.081	1.077
R_1[a] [$I = 2\sigma(I)$]	0.0335	0.0391	0.0358	0.0841	0.0201	0.0190
wR_2[a] (all data)	0.1050	0.1022	0.1089	0.2498	0.0500	0.0446

[a] $R_1 = \sum||F_o|-|F_c||/\sum|F_o|$; $wR_2 = [\sum w(F_o^2-F_c^2)^2/\sum w(F_o^2)^2]^{1/2}$.

1095 s, 1038 m, 1003 s, 880 m, 657 s. Elemental analysis for **2** · I: $C_2H_2N_3ZnI$ ($M_r = 260.34$). Calcd: H 0.77%, C 9.23%, N 16.14%. Found: H 0.71%, C 9.32%, N 16.50%.

2.3. X-ray crystallography

Diffraction data of **1** and **2** · *X* (*X* = Br, I) were collected on a Bruker SMART diffractometer with graphite monochromated Mo *K*α radiation ($\lambda = 0.71073$ Å) in φ and ω scan modes at 273 K. Absorption correction were applied by using the SADABS program [26]. The structure was solved by direct methods and successive Fourier difference syntheses (SHELXS-97), anisotropic thermal parameters for all nonhydrogen atoms were refined by full-matrix least-squares procedure on F^2 (SHELXTL-97) [27,28]. Hydrogen atoms were placed in geometrically calculated positions. Crystal data and details on refinements for complexes are summarized in Table 1. Selected bond distances and angles are listed in Table 2.

3. Results and discussion

3.1. Syntheses and PXRD

Metal-triazole-based materials have received considerable attention in the last decades, however, the polymeric phases generally occur as insoluble polycrystalline powders. Undoubtedly, the hydrothermal synthesis affords a convenient method for preparation of such composite materials, allowing more routine structural characterization by single crystal X-ray diffraction [18,19].

Different from **1** · Cl, **1** · Br and **1** · I failed to be prepared from the Hatcz ligand. Despite repeated attempts, no conditions were found to provide the target (see scheme S1). Considering being readily decarboxylated to form Hatrz under hydrothermal conditions [29], 3-amino-5-carboxyl-1,2,4-triazole (H_2atc) was employed in the construction of $[Zn(atrz)Br]_\infty$. As effective as hoped, $[Zn(atrz)Br]_\infty$ was successfully obtained from in-situ decarboxylation of H_2atc although the reactive mechanism in hydrothermal conditions was not clear. Decarboxylation was also observed for the related ligand 1H-1,2,4-triazole-3-carboxylic acid, under similar reaction conditions [30].

Similar to the previously described compounds [18,19], it is for all compounds in this study that the triazole-based ligand are present in the deprotonated form and serve as tridentate bridging group [31,32]. Compared with those in literatures [19,23], we provided a more convenient and wild condition for the syntheses of **2** · Cl and **2** · Br in this study.

The synthesized products of **1** and **2** · *X* (*X* = Br, I) were also characterized by PXRD. As shown in Fig. S1, the PXRD patterns are very consistent with the simulated results from single crystal data, illuminating the high purity of the as-synthesized samples.

3.2. Structure description

In the framework of **1**, Zn^{II} ion features a distorted tetrahedral geometry by three atrz nitrogen atoms (N1, N2, and N4) and one terminal *X* anion, as shown in Fig. 2S. The building blocks of the structures are constructed from binuclear planar $Zn_2(atrz)_2$ subunits depicted in Fig. 1, in which two Zn^{II} ions defined by the N1, N2 atoms from two different atrz ligands, and the separations of $Zn^{II}\cdots Zn^{II}$ are given in Table 3. As observed in Fig. 2, as three-connected nodes, μ_3-atrzs are connected with three Zn^{II} ions to generate a 2D isoreticular layer structure. The layers are further stacked in an ABAB sequence along the [001] direction, which is visualized by the translucent blue plane.

Apparently, both of Zn^{II} and atrz ions within a sheet are exhibiting three-connected nodes. The layer is extended through the N4 atoms connecting with Zn^{II} ions of the adjacent subunits, resulting in sixteen-membered tetranuclear $Zn_4N_8C_4$ cavities occupied by two amino groups from atrz ligands, which exhibits (4,4) topologic grid when the subunit is simplified as four-connected nodes, as shown in Fig. 2. Since Zn^{II} ions adopt tetrahedral coordination geometry and the remainder positions are occupied by the terminal *X* anions, the layers are not planar but rather corrugated. *X* anion pointing to either side of the layer act as both spacer and counter anion (see Fig. S3). When employing the various *X* anions, the average interlayer separations of **1** are gradually enlarged with the sequence of **1** · Cl, **1** · Br, **1** · I and **1** · SCN · H_2O, which equal to 5.851, 6.153, 6.651 and 8.292 Å. As anticipated, H_2O molecules reside in the spaces between two adjacent layers in **1** · SCN · H_2O, shown in Fig. 3.

Table 2
Selected bond lengths (Å) and angles (°) for compounds **1**, **2** · Br and **2** · I[a]

*$C_2H_3N_4ZnCl$ (**1** · Cl)*					
N(2)–Zn(1)#1	2.006(4)	Zn(1)–N(1)#2	1.998(4)	Zn(1)–N(4)	2.009(3)
Zn(1)–Cl(1)	2.2188(15)				
C(1)–N(2)–Zn(1)#1	127.9(3)	N(1)–N(2)–Zn(1)#1	125.9(3)	N(1)#2–Zn(1)–N(2)#3	108.25(15)
N(1)#2–Zn(1)–N(4)	107.91(15)	N(2)#3–Zn(1)–N(4)	107.85(15)	N(1)#2–Zn(1)–Cl(1)	114.43(13)
N(2)#3–Zn(1)–Cl(1)	110.68(12)	N(4)–Zn(1)–Cl(1)	107.50(12)	C(2)–N(1)–Zn(1)#4	128.6(3)
N(2)–N(1)–Zn(1)#4	125.4(3)	C(1)–N(4)–Zn(1)	131.4(3)	C(2)–N(4)–Zn(1)	125.8(3)
*$C_2H_3N_4ZnBr$ (**1** · Br)*					
Zn(1)–N(1)#1	1.998(5)	Zn(1)–N(2)	2.005(5)	Zn(1)–N(3)#2	2.011(5)
Zn(1)–Br(1)	2.3489(11)				
N(1)#1–Zn(1)–N(2)	107.94(19)	N(1)#1–Zn(1)–N(3)#2	107.62(19)	N(2)–Zn(1)–N(3)#2	107.36(19)
N(1)#1–Zn(1)–Br(1)	114.94(15)	N(2)–Zn(1)–Br(1)	110.78(14)	N(3)#2–Zn(1)–Br(1)	107.90(13)
C(2)–N(1)–Zn(1)#1	128.5(4)	N(2)–N(1)–Zn(1)#1	125.6(4)	C(1)–N(2)–Zn(1)	127.5(4)
N(1)–N(2)–Zn(1)	125.9(3)	C(2)–N(3)–Zn(1)#3	126.0(4)	C(1)–N(3)–Zn(1)#3	130.9(4)
*$C_2H_3N_4ZnI$ (**1** · I)*					
N(1)–Zn(1)#1	2.016(6)	N(3)–Zn(1)#2	2.023(5)	Zn(1)–N(1)#1	2.016(6)
I(1)–Zn(1)	2.5434(9)				
C(1)–N(1)–Zn(1)#1	127.6(5)	N(2)–N(1)–Zn(1)#1	126.0(4)	C(1)–N(3)–Zn(1)#2	131.2(4)
C(2)–N(3)–Zn(1)#2	125.6(5)	N(2)–Zn(1)–N(1)#1	107.3(2)	N(2)–Zn(1)–N(3)#3	106.6(2)
N(1)#1–Zn(1)–N(3)#3	107.9(2)	N(3)#3–Zn(1)–I(1)	107.93(15)	N(1)#1–Zn(1)–I(1)	111.28(14)
*$C_{12}H_{11}N_{20}S4Zn4O$ (**1** · SCN · H_2O)*					
N(9)–Zn(1)	1.934(13)	N(1)–Zn(1)	1.967(10)	N(3)#1–Zn(1)	1.988(9)
Zn(1)–N(5)	1.974(10)	Zn(2)–N(10)	1.926(12)	Zn(2)–N(2)	1.983(9)
Zn(2)–N(6)	1.988(9)	Zn(2)–N(7)#2	1.997(9)		
N(9)–Zn(1)–N(1)	110.1(5)	N(9)–Zn(1)–N(3)#1	107.4(5)	N(9)–Zn(1)–N(5)	109.0(4)
N(1)–Zn(1)–N(5)	113.8(5)	N(5)–Zn(1)–N(3)#1	108.4(4)	N(10)–Zn(2)–N(2)	114.6(5)
N(10)–Zn(2)–N(6)	111.8(5)	N(2)–Zn(2)–N(6)	109.1(4)	N(10)–Zn(2)–N(7)#2	106.5(5)
N(2)–Zn(2)–N(7)#2	106.3(4)	N(6)–Zn(2)–N(7)#2	108.2(4)		
*$C_2H_2N_3ZnBr$ (**2** · Br)*					
Zn(1)–N(2)#1	2.007(2)	Zn(1)–N(1)	2.009(2)	Zn(1)–N(3)#2	2.016(2)
Zn(1)–Br(1)	2.3453(5)				
N(2)#1–Zn(1)–N(1)	106.88(9)	N(2)#1–Zn(1)–N(3)#2	109.19(10)	N(1)–Zn(1)–N(3)#2	106.06(10)
N(2)#1–Zn(1)–Br(1)	114.95(7)	N(1)–Zn(1)–Br(1)	112.48(7)	N(3)#2–Zn(1)–Br(1)	106.92(7)
C(1)–N(1)–Zn(1)	125.39(19)	N(2)–N(1)–Zn(1)	128.79(18)	C(2)–N(2)–Zn(1)#1	129.72(19)
N(1)–N(2)–Zn(1)#1	123.98(18)	C(1)–N(3)–Zn(1)#3	125.04(19)	C(2)–N(3)–Zn(1)#3	131.74(19)
*$C_2H_2N_3ZnI$ (**2** · I)*					
Zn(2)–N(1)#3	2.007(3)	N(2)–Zn(2)#2	2.010(3)	Zn(2)–N(3)	2.021(3)
I(1)–Zn(2)	2.5329(5)				
C(1)–N(1)–Zn(2)#1	130.4(2)	N(2)–N(1)–Zn(2)#1	123.4(2)	C(2)–N(2)–Zn(2)#2	124.8(2)
N(1)–N(2)–Zn(2)#2	129.2(2)	N(1)#3–Zn(2)–N(2)#4	106.86(11)	N(1)#3–Zn(2)–N(3)	108.22(11)
N(2)#4–Zn(2)–N(3)	105.26(11)	N(1)#3–Zn(2)–I(1)	116.34(8)	N(2)#4–Zn(2)–I(1)	111.72(8)
N(3)–Zn(2)–I(1)	107.85(8)	C(2)–N(3)–Zn(2)	124.4(2)	C(1)–N(3)–Zn(2)	132.3(2)

[a] Symmetry transformations used to generate equivalent atoms: **1** · Cl. #1 $x+1/2, -y+1/2, -z+1$; #2 $-x+1/2, y-1/2, z$; #3 $x-1/2, -y+1/2, -z+1$; #4 $-x+1/2, y+1/2, z$. **1** · Br. #1 $-x+2, -y, -z+1$; #2 $x+1/2, -y+1/2, -z+1$; #3 $x-1/2, -y+1/2, -z+1$. **1** · I. #1 $-x+2, -y+2, -z$; #2 $x-1/2, -y+3/2, -z$; #3 $x+1/2, -y+3/2, -z$. **1** · SCN · H_2O. #1 $x,-y+1, z-1/2$; #2 $x,-y, z+1/2$. **2** · Br. #1 $-x, -y+1, -z+1$; #2 $x-1/2, -y+3/2, z-1/2$ #3 $x+1/2, -y+3/2, z+1/2$. **2** · I. #1 $-x+1/2, y+1/2, -z+1/2$; #2 $x-1/2, -y+3/2, z-1/2$; #3 $-x+1/2, y-1/2, -z+1/2$; #4 $x+1/2, -y+3/2, z+1/2$.

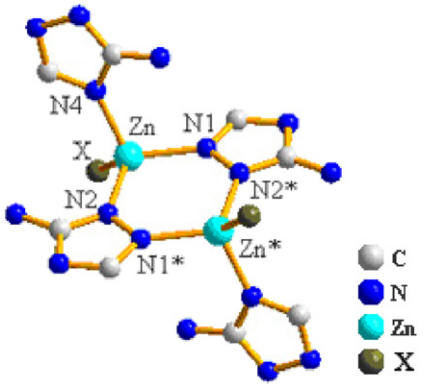

Fig. 1. The secondary building unit $Zn_2(atrz)_2$ in **1** (*symmetrically generated).

2 · *X* (*X* = Cl [23], Br [19], I) are isomorphous structures to **1** · *X*. In three isoreticular layer compounds based on binuclear planar Zn^{II} building blocks (see Fig. 4), Zn^{II} ion ligated by three μ_3-trz nitrogen atoms (N1, N2, and N4) and one terminal *X* anion (see Fig. S4) exhibits a distorted tetrahedral geometry and trz anions serve as the linkers of the structures.

Table 3
Relevant Zn···Zn distances (Å) for the 1 · *X* and 2 · *X* of this study (*X* = Cl^-, Br^-, I^-)

Compound	Zn···Zn	Compound	Zn···Zn
1 · Cl	3.7316(7)	**2** · Cl [23]	3.7588(19)
1 · Br	3.7400(11)	**2** · Br	3.7595(5)
1 · I	3.7631(9)	**2** · I	3.7653(6)

The structure of **2** · *X* also display (4,4) topologic motif, and the layers are stacked in an ABAB sequence along the [100] direction, which is visualized by the translucent laurel-green plane (see Fig. 5). Different with **1**, $Zn_4N_8C_4$ rings are formed within the layer in **2** · *X* just because unsubstituted μ_3-trz anions act as the linkers, as shown in Figs. 5 and 6. The dimension of the ring is approximately 3.32 × 3.17 Å, considering the van der Waals

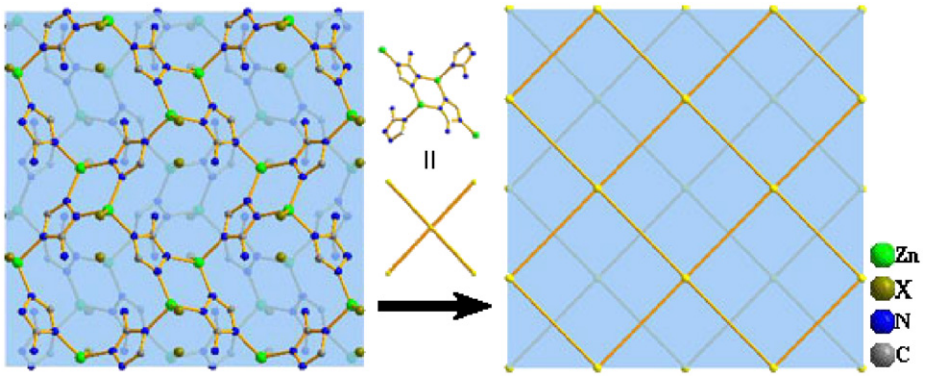

Fig. 2. The ABAB sequence stacking representation of the 2D layer structure of **1** viewed along the *c*-axis direction. $X = Cl^-$, Br^-, I^- (left, entity of the layer; right, its topologic illustration).

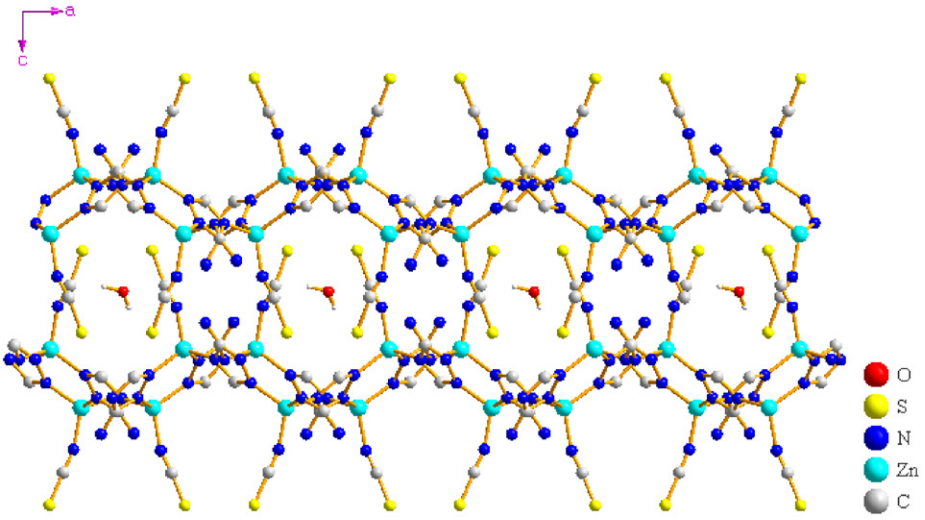

Fig. 3. View of the 2D layer structure of $\mathbf{1}\cdot SCN\cdot H_2O$ along the *b*-axis direction.

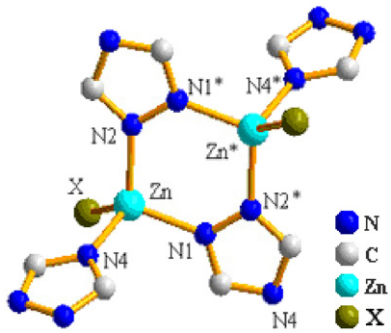

Fig. 4. The secondary building unit $Zn_2(atrz)_2$ in **2** (* symmetrically generated).

radii of Zn atoms [33]. The average interlayer separations are also gradually enlarged by changing the terminal counteranions with the sequence of Cl^-, Br^-, I^-, which are 5.701 [23], 5.764 and 6.280 Å, respectively.

It should be stressed that the orientation of the Zn–*X* bonds in such structures provides an accumulation of negative charges between the layers. Such charges polarization could lead to an interesting interaction of Zn(trz)*X* or Zn(atrz)*X* with polar species hold in the free spaces between two adjacent layers. Therefore, how to construct the targeted compounds is the critical factor. Why does $\mathbf{1}\cdot SCN\cdot H_2O$ contain H_2O molecules while the others do not? Obviously, $\mathbf{1}\cdot SCN\cdot H_2O$ is the representative example to exemplify the reason. Compared with $\mathbf{1}\cdot SCN\cdot H_2O$, it comes to the conclusions for $\mathbf{1}\cdot X$ that either the interlayer separations are too strait, or the $Zn_4N_8C_4$ rings are occupied, or both cases concur, excludes the guest molecules from such frameworks.

As shown in Fig. S5, the interlayer separations of Cu(trz) and Ag(trz) [24] are too strait to contain H_2O molecules, since the 2D networks provide potential $\pi\cdots\pi$, $M\cdots\pi$, and $M\cdots M$ (M = Cu, Ag) interactions for crystal packing, and the very short average plane-to-plane separations are 3.105 and 3.028 Å, respectively. As for Zn(dmtrz)Cl and Cd(datrz)I [25], shown in Fig. S6, the existence of four-coordinated Zn^{II} and Cd^{II} ions destroys the $\pi\cdots\pi$, $M\cdots\pi$, and $M\cdots M$ interactions described in former, and the introduced terminal anions Cl^- and I^- as spacers evidently enlarge the layer separations as 6.775 and 7.512 Å, respectively. However, tetranuclear $Zn_4N_8C_4$ rings are occupied by four NH_2 and CH_3 groups from dmtrz and datrz ligands, especially the dmtrz and datrz within layers are not coplanar but rather corrugated, which means that NH_2 and CH_3 groups occupy spaces between two adjacent layers to a certain extent, decreasing the available spaces which could hold the guest molecules, potentially. In order to solve the issues, Hatrz, Htrz, and Zn^{II} were employed to construct the simplified isoreticular layers, and *X* ($X = Cl^-$, Br^-, I^-, SCN^-) as

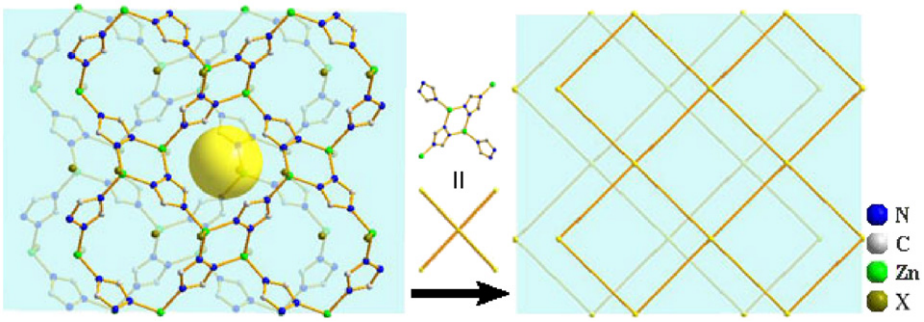

Fig. 5. Structural and topologic illustrations of **2** viewed along the *c*-axis direction. $X = Cl^-$, Br^-, I^-.

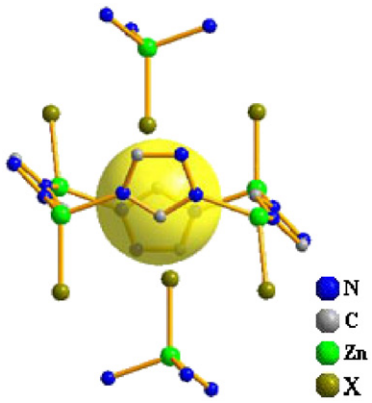

Fig. 6. Perspective view of the cavity encircled by $Zn_4N_8C_4$ ring (inner cavity are highlighted as a translucent yellow sphere).

the terminal counter anion and spacer to enlarge the average interlayer separation. Ultimately, it is as anticipated that $\mathbf{1}\cdot SCN\cdot H_2O$ was obtained.

3.3. Luminescence property

Polymeric complexes of metal cations with the d^{10} configuration, such as Cu(I), Ag(I), Au(I) [19,34–40], Zn(II), and Cd(II) [25,41–43], and polyazaheterocyclic ligands have been shown to possess interesting luminescent properties. The emissions observed for materials of the Zn(II)/dmtrz (dmtrz = 3,5-dimethyl-1,2,4-triazole) [25] and Zn(II)/trz [19], Zn(II)/tetrazolyl [42] classes were assigned as originating from the ligand-to-metal charge transfer (LMCT) and intraligand π–π^* transitions, respectively.

The solid-state luminescence properties of compounds **1**, $\mathbf{2}\cdot I$ as well as the Hatrz (3-amino-1H-1,2,4-triazole) ligand upon the radiation of UV light in the polycrystalline state were investigated at room temperature. As shown in Fig. 7, all compounds in this study with the exception of $\mathbf{2}\cdot I$ exhibit strong emission in high-energy region. The free Hatrz ligand shows two intense fluorescent emission bands at $\lambda_{max} = 390$, 363 nm under 242, 278 nm excitation, respectively, shown in Fig. 8, while Htrz (1H-1,2,4-triazole) exhibits only a fluorescent emission band at $\lambda_{max} = 421$ nm under 318 nm excitation [19]. The photoluminescence of Hatrz and Htrz have been assigned as originating from π–π^* transitions. Upon complexion of both Hatrz and *X* anions ($X = Cl^-$, Br^-, I^-, SCN^-) with the Zn(II) ion, compound $\mathbf{1}\cdot Cl$, shown in Fig. 9, displays two strong fluorescence emission bands at $\lambda_{max} = 383$, 349 nm ($\lambda_{ex} = 253$, 280 nm) and each complex of $\mathbf{1}\cdot Br$, $\mathbf{1}\cdot I$ and $\mathbf{1}\cdot SCN\cdot H_2O$ displays only a emission band (see Table 4). These emission bands are neither metal-to-ligand charge transfer (MLCT) nor LMCT in nature, but rather can be attributed to an intraligand emission state, because very similar emissions are also observed for the free Hatrz ligand. For comparison, the maximum emission of complexes $\mathbf{1}\cdot Cl$, $\mathbf{1}\cdot Br$, and $\mathbf{1}\cdot I$ excited at the similar wavelengths 280 and 290 nm are red-shifted and weaken in sequence. The same phenomenon also exhibit in the maximum emission of complexes $\mathbf{1}\cdot Cl$ and $\mathbf{1}\cdot SCN\cdot H_2O$ excited at 253 and 243 nm, which are probably due to the differences of the terminal counteranions and the coordination environment around the metal ions because the photoluminescence behavior is closely associated with the central metal ion and the coordination ligand.

As for compound $\mathbf{2}\cdot I$, there is near nonfluorescent in the range 400–800 nm for excitation wavelengths between 200 and 400 nm. The chloride and bromide analogues $\mathbf{2}\cdot Cl$ and $\mathbf{2}\cdot Br$ ($[Zn(trz)Cl]_\infty$ and $[Zn(trz)Br]_\infty$) were investigated by Ouellette et al. via solid-state density functional theory (DFT) calculations [19]. The absence of photoluminescence for the bromide analogue $\mathbf{2}\cdot Br$ ($[Zn(trz)Br]_\infty$) with the exception of $[Zn(trz)Cl]_\infty$ was observed, which suggests that iodide and bromide analogues possess a greater vibrational density of state which provides more effective radiationless relaxation for these material than in the case of the chloride analogue.

3.4. Thermal analysis

As shown in Fig. S7 for $\mathbf{1}\cdot X$ and $\mathbf{2}\cdot X$ ($X = Cl^-$, Br^-, I^-), the thermal decomposition profiles are generally quite similar to each other according to the *X* anion, obviously, which is consistent with their isomorphism substructure skeleton. The polymers are thermally stable up to 430, 480, 490 °C for $\mathbf{1}\cdot X$ and 420, 475, 490 °C for $\mathbf{2}\cdot X$, respectively. Then, there are initial weight losses following which are supposed as the whole architecture decomposition processes. These processes are associated with the losses of the organic ligand and *X* anion to leave the residue of ZnO (exp. 44.19%, 35.23%, and 29.31%, calcd. 44.25%, 35.64%, and 29.56% for $\mathbf{1}\cdot X$; exp. 48.12%, 38.10%, and 31.15%, calcd. 48.19%, 38.15%, and 31.26% for $\mathbf{2}\cdot X$).

Upon heating polymer $\mathbf{1}\cdot SCN\cdot H_2O$ up to 343 °C there is no mass loss observed, and further heating the water molecules are released (mass loss: exp. 8.17%; calcd. 8.02%), in the temperature interval 343–425 °C, shown in Fig. S8. Like the others above, the dehydrated species ($\mathbf{1}\cdot SCN$) followed one-step weight loss in the temperature interval 425–725 °C, corresponding to the decomposition of organic components and SCN^-, respectively. The whole weight loss 61.86% is in accordance with the expected value 62.71%. The thermogravimetric analysis results show that these coordination polymers exhibit high thermal stability.

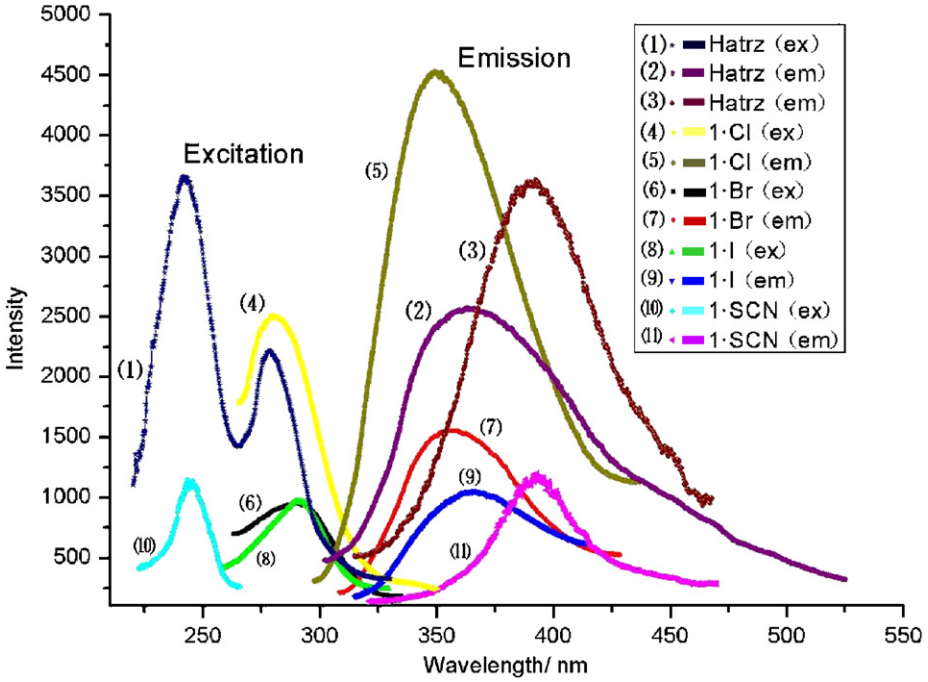

Fig. 7. Excitation and emission spectra of $\mathbf{1}\cdot X$ ($X = Cl^-$, Br^-, I^-), $\mathbf{1}\cdot SCN\cdot H_2O$ and Hatrz in the solid state at room temperature.

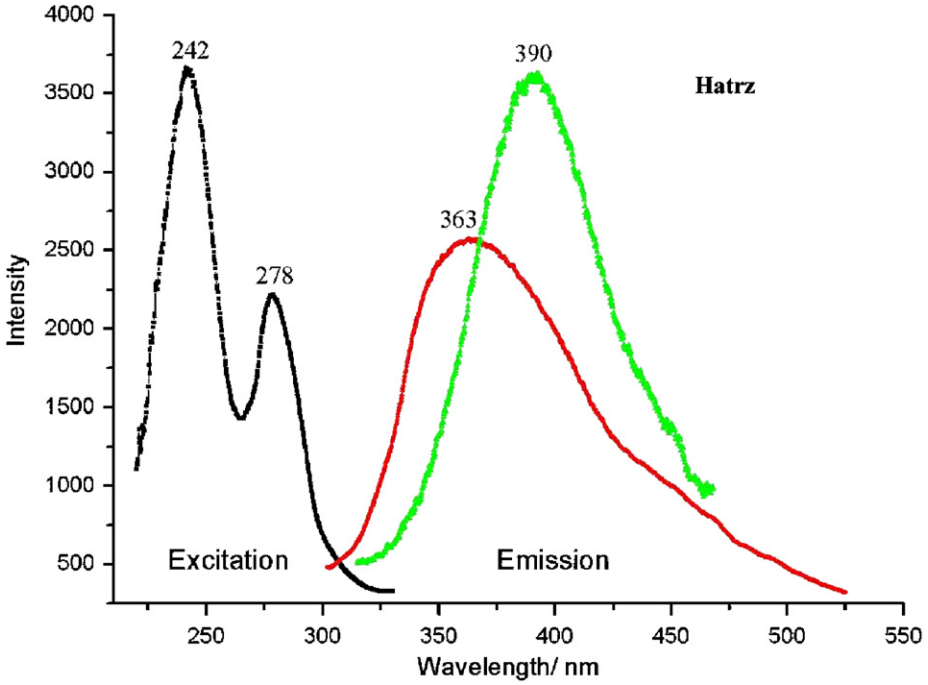

Fig. 8. Excitation and emission spectra of Hatrz ligand in the solid state at room temperature. Strong emission at $\lambda_{max} = 390$, 363 nm upon excitation at $\lambda_{ex} = 242$, 278 nm, correspondingly.

4. Conclusions

Two types of 2D isoreticular layers of coordination polymers $[Zn(atrz)X]_\infty$ ($X = Cl^-$, Br^-, I^-), $Zn_4(atrz)_4(SCN)_4\cdot H_2O$ and $[Zn(trz)X]_\infty$ ($X = Cl^-$, Br^-, I^-) have been constructed under hydrothermal conditions. Both of them display (4,4) topologic motif. In all cases, Zn^{II} cations and atrz or trz anions construct the grids within the layers, and the terminal ions X act as both spacers and counteranions. The isoreticular layers are stacked in an ABAB sequence. Based in employing the various terminal counteranions X ($X = Cl^-$, Br^-, I^-, SCN^-), the average interlayer separations were enlarged, and guest molecules H_2O reside in the spaces between two adjacent layers of $[Zn_4(atrz)_4(SCN)_4\cdot H_2O]_\infty$, eventually. It is presumed that the isomorphous structure of $[Zn(trz)X]_\infty$ ($X = SCN^-$, N_3^-) would provide much available room for holding guest molecules. We are presently exploring this possibility. The thermogravimetric analyses results show that these coordination polymers exhibit high thermal stability. Furthermore, the photoluminescence associated with many d^{10} complexes encouraged us to study the optical properties of the materials obtained in this

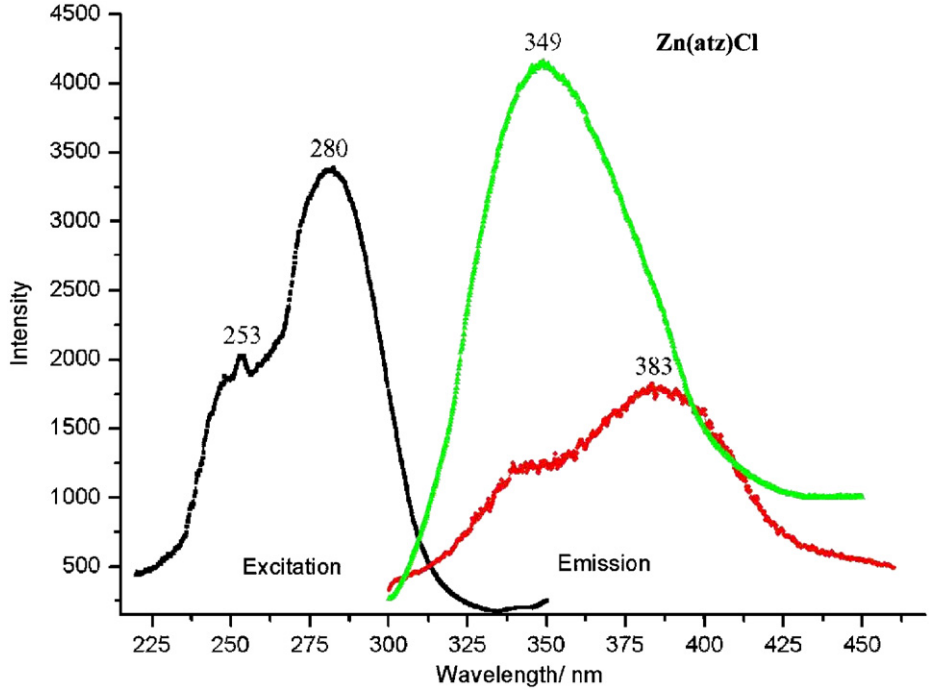

Fig. 9. Excitation and emission spectra of complex **1**·Cl in the solid state at room temperature. Strong emission at $\lambda_{max} = 349$, 383 nm upon excitation at $\lambda_{ex} = 280$, 253 nm, correspondingly.

Table 4
Excitation and emission data of compounds Htrz, Hatrz and **1**

Compound	λ_{ex} (nm)	λ_{max} (nm)	Possible origin
Htrz	318	421	π–π^*
Hatrz	242	390	π–π^*
	278	363	π–π^*
1·Cl	253	383	π–π^*
	280	349	π–π^*
1·Br	290	355	π–π^*
1·I	290	366	π–π^*
1·SCN·H_2O	243	393	π–π^*

study. All of the complexes in the solid state with the exception of **2**·I exhibit strong fluorescent emission bands, which presumably arise from the ligand π–π^* transition.

Supplementary material

Crystallographic data for the four complexes in this paper have been deposited at the Cambridge Crystallographic data center, CCDC Nos. 624838, 631429, 633360, 641406, 633359 and 635131 are for complexes **1**·X ($X = Cl^-$, Br^-, I^-), **1**·SCN·H_2O and **2**·X ($X = Br^-$, I^-), respectively. These data can be obtained free of charge at http://www.ccdc.cam.ac.uk/conts/retrieving-.html (or from the Cambridge Crystallographic Data Center, 12 Union Road, Cambridge CB2 1EZ, UK; fax: +44 1223 336 033; e-mail: deposit@ccdc.cam.ac.uk).

Acknowledgments

The authors gratefully acknowledged the financial supports from the National Natural Science Foundation of China (Grant no. 20771089), the National Natural Science Foundation of Shaanxi Province (Grant no. 2007B02) Shaanxi Physico-chemical Key Laboratory, Shaanxi key Laboratory of Chemical Reaction Engineering and the Science and Technology Foundation of the National Defense Key Laboratory of Propellant and Explosive Combustion of China (Grant no. 51455010105QT3001).

Appendix A. Supplementary material

Supplementary data associated with this article can be found in the online version at doi:10.1016/j.jssc.2008.08.027.

References

[1] C. Janick, Dalton Trans. (2003) 2781–2804 and references therein.
[2] S. Kitagawa, S. Noro, Compr. Coord. Chem. II 7 (2004) 231.
[3] O.M. Yaghi, M. O'Keeffe, N.W. Ockwig, H.K. Chae, M. Eddaoudi, J. Kim, Nature 423 (2003) 705–714.
[4] S.L. James, Chem. Soc. Rev. 32 (2003) 276–288.
[5] C.N.R. Rao, S. Natarajan, R. Vaidhyanathan, Angew. Chem., Int. Ed. 43 (2005) 1466–1496.
[6] S. Kitagawa, R. Kitaura, S.I. Noro, Angew. Chem., Int. Ed. 43 (2004) 2334–2375.
[7] G.S. Papaefstathiou, L.R. MacGillivray, Coord. Chem. Rev. 246 (2003) 169–184.
[8] M. Eddaoudi, D.B. Moler, H. Li, B. Chen, T.M. Reineke, M. O'Keeffe, O.M. Yaghi, Acc. Chem. Res. 34 (2001) 319–330.
[9] R.C. Finn, R.C. Haushalter, J. Zubieta, Prog. Inorg. Chem. 51 (2003) 421–601.
[10] A. Vioux, J. LeBideau, P.H. Mutin, D. Leclercq, Top. Curr. Chem. 232 (2004) 145–174.
[11] A. Clearfield, Curr. Opin. Solid State Mater. Sci. 6 (2003) 495–506.
[12] A. Clearfield, Prog. Inorg. Chem. 47 (1998) 371–510.
[13] G. Alberti, in: J.L. Atwood, J.E.D. Davis, F. Vogel (Eds.), Comprehensive Supramolecular Chemistry, vol. 9, Pergamon Press, New York, 1996; G. Alberti, T. Bein (Eds.), pp. 152–187.
[14] G. Ferey, Chem. Mater. 13 (2001) 3084–3098.
[15] U. Beckmann, S. Brooker, Coord. Chem. Rev. 245 (2003) 17–29.
[16] J.G. Haasnoot, Coord. Chem. Rev. 200 (2000) 131–185.
[17] M.H. Klingele, S. Brooker, Coord. Chem. Rev. 241 (2003) 119–132.
[18] J.-P. Zhang, X.-M. Chen, Chem. Commun. (2006) 1689–1699.
[19] W. Ouellette, B.S. Hudson, J. Zubieta, Inorg. Chem. 46 (2007) 4887–4904.
[20] W. Ouellette, A.V. Prosvirin, J. Valeich, K.R. Dunbar, J. Zubieta, Inorg. Chem. 46 (2007) 9067–9082.

[21] O.M. Yaghi, M. O'Keeffe, N.W. Ockwig, H.K. Chae, M. Eddaoudi, J. Kim, Nature 423 (2003) 705–714.
[22] W. Li, H.-P. Jia, Z.-F. Ju, J. Zhang, Cryst. Growth Des. 6 (2006) 2136–2140.
[23] J. Kröber, I. Bkouche-Waksman, C. Pascard, M. Thonmann, O. Kahn, Inorg. Chim. Acta 230 (1995) 159–163.
[24] J.-P. Zhang, Y.-Y. Lin, X.-C. Huang, X.-M. Chen, J. Am. Chem. Soc. 127 (2005) 5495–5506.
[25] Q.-G. Zhai, X.-Y. Wu, S.-M. Chen, C.-Z. Lu, W.-B. Yang, Cryst. Growth Des. 6 (2006) 2126–2135.
[26] G.M. Sheldrick, SADABS. Software for Empirical Absorption Corrections, University of Gottingen, Germany, 2000.
[27] G.M. Sheldrick, SHELXS-97, Program for Solution of Crystal Structures, University of Göttingen, Göttingen, Germany, 1990.
[28] G.M. Sheldrick, SHELXL-97, Program for Refinement of Crystal Structures, University of Göttingen, Göttingen, Germany, 1997.
[29] C.-Y. Su, A.M. Goforth, M.D. Smith, P.J. Pellechia, H.-C. zur Loye, J. Am. Chem. Soc. 126 (2004) 3576–3586.
[30] D.W. Wiley, O.W. Webster, E.P. Blanchard, J. Org. Chem. 41 (1976) 1891–1895.
[31] D.J. Chesnut, A. Kusnetrzow, R. Birge, J. Zubieta, Inorg. Chem. 38 (1999) 5484–5494.
[32] Deprotonation of the 1,2,4-triazole ligand ($pKa = 2.25$) is found to be a common feature of its hydrothermal chemistry in the presence of metals, and a shift in pKa is found to occur under hydrothermal conditions [28]. Therefore, it is understandable that Hatrz ($pKa = 4.04$) takes the deprotonated form to participate in metal ion coordination under slightly acidic reaction conditions. The pH of a typical reaction mixture before reaction is about 4. The use of Hatc may give a more acidic reaction mixture, but because it undergoes decarboxylation to become Hatrz, deprotonation is still expected.
[33] A. Bondi, J. Phys. Chem. 68 (1964) 441–451.
[34] H.V.R. Dias, H.V.K. Diyabalanage, M.G. Eldabaja, O. Elbjeirami, M.A. Rawashdeh-Omary, M.A. Omary, J. Am. Chem. Soc. 127 (2005) 7489–7501.
[35] M.A. Omary, M.A. Rawashdeh-Omary, M.W.A. Gonser, O. Elbjeirami, T. Grimes, T.R. Cundair, Inorg. Chem. 44 (2005) 8200–8210.
[36] A.O. Mohammad, A.R.O. Manal, V.K.D. Himashinie, H.V. Rasika Dias, Inorg. Chem. 44 (2003) 8612–8614.
[37] W. Ouellette, A.V. Prosvirin, V. Chieffo, K.R. Dunbar, B. Hudson, J. Zubieta, Inorg. Chem. 45 (2006) 9346–9366.
[38] C.-M. Che, H.-Y. Chao, V.M. Miskowski, Y.-Q. Li, K.-K. Cheung, J. Am. Chem. Soc. 123 (2001) 4985–4991.
[39] W.-Y. Wong, L. Liu, J.-X. Shi, Angew. Chem., Int. Ed. 42 (2003) 4064–4068.
[40] M. Enomoto, A. Kishimura, T. Aida, J. Am. Chem. Soc. 123 (2001) 5608–5609.
[41] B. Ding, L. Yi, Y. Wang, P. Cheng, D.-Z. Liao, S.-P. Yan, Z.-H. Jiang, H.-B. Song, H.-G. Wang, Dalton Trans. (2006) 665–675.
[42] X.-S. Wang, Y.-Z. Tang, X.-F. Huang, Z.-R. Qu, C.-M. Che, P.W.H. Chan, R.-G. Xiong, Inorg. Chem. 44 (2005) 5278–5285.
[43] X. He, C.-Z. Lu, D.-Q. Yuan, Inorg. Chem. 45 (2006) 5760–5766.